Journal of Tissue Engineering
Volume 9: 1–9

DOI: 10.1177/2041731418790315
journals.sagepub.com/home/tej
SAGE

Near-infrared laser-mediated drug release and antibacterial activity of gold nanorod–sputtered titania nanotubes

Kyoung-Suk Moon[1], Young-Bum Park[2], Ji-Myung Bae[1] and Seunghan Oh[1]

Abstract

The infection control of implants is one of the hot issues in the field of medicine and dentistry. In this study, we prepared gold nanorod–sputtered titania nanotubes on titanium surface, which is the main component of implant material, and aimed to estimate the remote-controlled tetracycline release and resulting antibacterial effects of gold nanorod–sputtered titania nanotubes using near-infrared laser irradiation. Gold nanorods prepared by ion plasma sputtering (aspect ratio = 1:3) showed optical properties like those of chemically synthesized gold nanorods, exhibiting photothermal effects in the near-infrared region, as demonstrated using field-emission scanning electron microscopy, transmission electron microscopy, and diffuse ultraviolet–visible–near-infrared spectrophotometry. In addition, a 2 wt% tetracycline/polycaprolactone mixture was found to be the most suitable experimental group to demonstrate the biological compatibilities and antibacterial activities. The results of antibacterial agar diffusion tests and near-infrared-mediated tetracycline release tests in vivo confirmed that remote-controlled tetracycline elution using near-infrared laser irradiation was highly effective. Therefore, gold nanorod–sputtered titania nanotubes would be expected to enable the continued use of the photothermal therapy of gold nanorods and extend the limited use of titania showing photocatalytic activity only within the ultraviolet-to-near-infrared region.

Keywords

Gold nanorods, titania nanotubes, near-infrared laser, tetracycline, antibacterial activity

Date received: 15 April 2018; accepted: 2 July 2018

Introduction

Bacterial infection is a frequent cause of peri-implantitis in the dental field and can cause a continuous inflammatory reaction that destroys the bonding of the implant and the bone.[1] Although sterilization methods, such as antimicrobial drugs, laser irradiation, and ozone treatment, are used to prevent bacterial infection, it is difficult to remove bacteria present in dental plaque, which acts as a strong protective layer, after implantation.[2] Recently, various studies have attempted to prevent plaque generation by coating the implant surface with a biodegradable polymer material containing an antibiotic.[3] Many studies have evaluated remote-controlled drug elution by near-infrared (NIR) laser irradiation, but most of the studies are related to the development of nanocarriers including drugs for tumor therapy.[4–7]

Gold nanorods (GNRs) have a surface plasmon resonance (SPR) band in the NIR region that is converted into heat via the photothermal effect.[8] SPR causes resonance of an electromagnetic wave with a specific wavelength depending on the shape, size, and type of metal and strongly

[1]Department of Dental Biomaterials and Institute of Biomaterial and Implant, College of Dentistry, Wonkwang University, Iksan, Republic of Korea
[2]Department of Prosthodontology, College of Dentistry, Yonsei University, Seoul, Republic of Korea

Corresponding author:
Seunghan Oh, Department of Dental Biomaterials and Institute of Biomaterial and Implant, College of Dentistry, Wonkwang University, Iksan 54538, Jeonbuk, Republic of Korea.
Email: shoh@wku.ac.kr

absorbs the wavelength through collective oscillation of conduction electrons on the metal surface. With such strong absorption, GNRs can be applied for photothermal therapy, which uses heat generation.[9] By exploiting the properties of GNRs, selective drug elution may be possible using NIR laser remote control in the clinical setting.[10–12] However, few studies have evaluated this potential application of GNRs owing to difficulties in GNR mass production, the lack of studies related to implant surface applications, and expensive production costs. Although it is easy to synthesize small amounts of GNRs by seed-mediated techniques based on chloroauric acid ($HAuCl_4$), it is difficult to prepare large amounts of GNRs by chemical synthesis, as required to produce GNR-coated titanium implants. As reported in our previous study,[13] GNR (12.23 ± 0.73 wt%)-grafted titania (TiO_2) nanotubes were prepared by thiolactic acid surface treatment. However, it was impossible to coat more than 13 wt% GNRs to the surface of TiO_2 nanotubes based on thiolactic acid surface treatment. Thus, novel implant surface coating technologies using GNRs are needed to overcome this drawback of the conventional methods for synthesizing GNRs and coating GNRs to TiO_2 nanotubes.

Therefore, in this study, we attempted to deposit GNRs on TiO_2 nanotubes by ion plasma sputtering to maximize the photothermal effects of GNRs by NIR laser irradiation. TiO_2 nanotubes are known to show superhydrophilicity, thereby accelerating initial cell attachment, proliferation, and osseointegration;[14–17] and thus the combination of GNRs and TiO_2 nanotube is expected to be applicable for surface treatment of dental implants. The aims of this study were to prepare GNR-sputtered TiO_2 nanotubes (designated GNRs-TiO_2 nanotubes), characterize the surface properties of GNRs-TiO_2 nanotubes, and evaluate NIR laser–mediated drug release and antibacterial activity of tetracycline (TC)/polycaprolactone (PCL)-coated GNRs-TiO_2 nanotubes.

Materials and methods

Preparation of GNRs-TiO_2 nanotubes

As reported previously,[18] a commercial pure titanium sheet (250 μm thick, 5×5 cm^2, 99.5%; Hyundai Titanium Co., South Korea) was cleaned with ethyl alcohol (99.5%, Sigma, USA) and double-distilled water. TiO_2 nanotubes measuring 100 nm in diameter were anodized in 0.5 w/v% hydrofluoric acid (48 w/v%; Merck, USA) aqueous solution at 20 V for 30 min. A platinum electrode (99.99%, *DSM* Co., South Korea) served as the counterpart. The anodized TiO_2 nanotubes were then rinsed with double-distilled water, dried at 60°C overnight, and heat-treated at 400°C for 3 h (in air, heating and cooling rates = 1°C/min) to prepare crystallized TiO_2 nanotubes.

GNRs-TiO_2 nanotubes were prepared using direct current (DC) plasma sputter (Cressington 108; Cressington Scientific Instruments, UK). Gold sputtering was performed at the applied voltage of 10 mA under vacuum conditions of less than 0.1 mbar for 1, 3, 5, and 7 min to determine the optimal conditions showing maximum light observance in the NIR region (800–850 nm). Uncoated TiO_2 nanotubes were used as a control.

Surface characterization

Analyses of the morphology, elemental composition, and optical properties of GNRs-TiO_2 nanotubes were performed using field-emission scanning electron microscopy (FE-SEM; S4800S; Hitachi & Horiba Co., Japan), transmission electron microscopy (TEM; JEM-2100F; JEOL, Japan), energy-dispersive X-ray spectroscopy (EDX; Oxford Instruments Analytical 7582, UK), and diffuse reflectance ultraviolet–visible (UV-Vis) spectrophotometry (SolidSpec-3700; Shimadzu Scientific Co., Japan). Analysis of changes in the surface chemical composition was performed using X-ray photoelectron spectroscopy (XPS; K-alpha; Thermo, UK) equipped with a monochromatic A1 Kα source. The carbon, oxygen, gold, and titanium contents on the surface were measured to evaluate changes in surface chemistry before and after gold plasma coating. Survey scan spectra were obtained at a pass energy of 100 eV (step size: 1 eV), and detailed scan spectra were obtained at a pass energy of 50 eV (step size: 0.1 eV). The photoelectron binding energy was calibrated to the C1s (284.8 eV) peak.

Coating of GNRs-TiO_2 nanotubes with the PCL/TC mixture

A mixture of TC (Sigma) dissolved in dimethyl sulfoxide and PCL (Sigma) dissolved in tetrahydrofuran (Sigma) was stirred for 6 h. The concentrations of TC used in this study were 2, 4, and 5 wt%, and the concentration of PCL was 2 wt%. An amount of 100 μL of the mixed solution was coated onto the GNRs-TiO_2 nanotubes via an electrospinning device (ESR200R2; NanoNC, Korea). The rate of electrospinning was 20 μL/min.

Cell proliferation and 3-(4,5-dimethylthiazol-2-yl)-2,5-diphenyltetrazolium bromide cytotoxicity test

Fluorescein diacetate (FDA; Sigma) staining was performed to count viable human mesenchymal stem cells (hMSCs; Lonza, USA) adhered to the experimental specimen to estimate the degree of cell adhesion at the beginning of the incubation period. At 24 and 48 h after plating, hMSCs on the experimental specimens were rinsed with phosphate-buffered saline (PBS; Invitrogen, USA) and incubated with an FDA working solution (50 μg FDA dissolved in 10 mL PBS) for 30 s. FDA-stained specimens

were washed twice with PBS, and the washed specimens were viewed under an inverted fluorescence microscope (CKX41; Olympus Co., Japan). FDA-stained viable cells were counted in four areas for each specimen.

The 3-(4,5-dimethylthiazol-2-yl)-2,5-diphenyltetrazolium bromide (MTT) cytotoxicity tests were conducted to investigate the cytotoxicity of TC/PCL-coated GNRs-TiO_2 nanotubes with various concentrations of TC. The experimental specimens were washed with PBS and transferred to a new 12-well plate. Next, 1 mL MTT dye (Sigma) was added to each well. After 3 h of incubation in a 5% CO_2 incubator, 1 mL isopropanol was added to each well and the 12-well plate was then shaken for 30 min. The absorbance of each solution was measured at 570 nm with a microplate enzyme-linked immunosorbent assay reader (SpectraMax 250; Thermo Electron Co., USA). Data analysis for MTT assays was conducted using ISO 10993-5, Annex C.[19] If the cell viability was less than 70% of the blank, the specimen was considered to have cytotoxic potential.

Antibacterial agar diffusion test

Antibacterial agar diffusion test was conducted by modifying our previous experimental protocol.[13] *Streptococcus mutans* (ATCC 25176; ATCC, USA) was incubated in brain heart infusion broth (BHIB; Difco Co., USA) to test the antibacterial agar diffusion of TC/PCL-coated GNRs-TiO_2 nanotubes. When the bacteria had high confluence, 100 μL of the incubated solution was diluted to 10,000 CFU/mL and mixed with the agar medium. *S. mutans*-containing medium was seeded onto 100-mm tissue culture dishes and incubated at 37°C for 24 h to solidify the agar medium and form *S. mutans* colonies. Experimental specimens ($1 \times 1\ cm^2$) were placed onto the *S. mutans*-incubated agar medium, and NIR laser irradiation (power: 200 mW, wavelength: 830 nm; RaeHwa, Korea) was conducted for 1 min. After NIR laser irradiation, the specimen was removed from the bacteria-incubated agar medium to exclude the unwanted amounts of TC released from the specimen during the test, and the agar medium was stored at 37°C for 24 h. *S. mutans*-incubated agar medium without NIR laser irradiation was used as a control. After a second incubation period of 24 h, the zone diameters of *S. mutans* colonies were measured three times per specimen to minimize measurement error.

NIR laser–mediated TC release in vivo

NIR laser–mediated TC release in vivo was analyzed with the approval of the Wonkwang University Institutional Animal Care and Use Committee (WKU16-89). In this study, 4-week-old male Institute of Cancer Research (ICR) mice (body weight: 23–25 g; Damool Science, Korea) were used. For intraperitoneal insertion, a 1-cm incision in the abdominal cavity was made using scissors, and the endothelial space was secured. TC/PCL-coated GNRs-TiO_2 nanotubes were inserted into the abdominal cavity of the mouse. Next, NIR laser irradiation was conducted for 1 min. After 30 min of NIR laser irradiation, the mice were sacrificed and blood was collected. The supernatant (blood plasma) was collected from the blood samples by centrifugation (5000 r/min, 10 min) and stored at −80°C until subsequent analysis. Quantitative analysis of TC in mouse blood plasma was then performed by liquid chromatography–tandem mass spectrometry (LC-MS/MS; triple quadrupole tandem mass spectrometer; Agilent 6410 Triple Quadrupole; Agilent, USA). Four different concentrations of TC samples (1, 10, 100, and 1000 ng/mL) were also measured to quantify the released amount of TC from the mouse blood.

Data analysis

All data were expressed as means ± standard deviations. The data for MTT cytotoxicity tests and viable cell counts were analyzed statistically by one-way analysis of variance (SPSS 23.0; IBM SPSS, USA) and post hoc Duncan's multiple range tests. The data for antibacterial agar diffusion tests and NIR laser–mediated TC release in vivo were analyzed by paired *t* tests. Differences were considered significant if the *P* values were less than 0.05.

Results

Figure 1 shows a schematic diagram of the preparation of the TC/PCL-coated GNRs-TiO_2 nanotube drug release system. Figure 2 shows the FE-SEM images of GNRs-TiO_2 nanotubes with 1, 3, and 5 min of gold sputtering. Based on 50 gold nanoparticle measurements from the vertical view of Figure 2(d), the short axis, long axis, and aspect ratio of gold nanoparticles deposited onto TiO_2 nanotubes were 33.99 ± 3.75 nm, 100.40 ± 11.74 nm, and 2.96 ± 0.14, respectively. Thus, most of the deposited gold nanoparticles were vertically aligned on the top layer of TiO_2 nanotubes in the form of nanorods as the gold sputtering time increased.

Figure 3 shows the TEM images and EDX analysis of the vertically sectioned GNRs-TiO_2 nanotubes (after 5 min of gold coating). In Figure 3(a), gold was detected in the whole area of TiO_2 nanotubes, and most gold nanoparticles were observed in the uppermost layer of TiO_2 nanotubes. In addition, 5.03 wt% gold was detected in the mapped area of the TEM images based on EDX analysis.

Figure 4 shows the diffuse ultraviolet–visible–near-infrared (UV-Vis-NIR) spectra of GNRs-TiO_2 nanotubes with various gold sputtering periods. The electron absorption spectra of all GNRs-TiO_2 nanotubes showed four peaks at the wavelength (350–400 m, 400–450 nm, 500–600 nm, and 800–850 nm). Among four peaks, two absorption peaks at

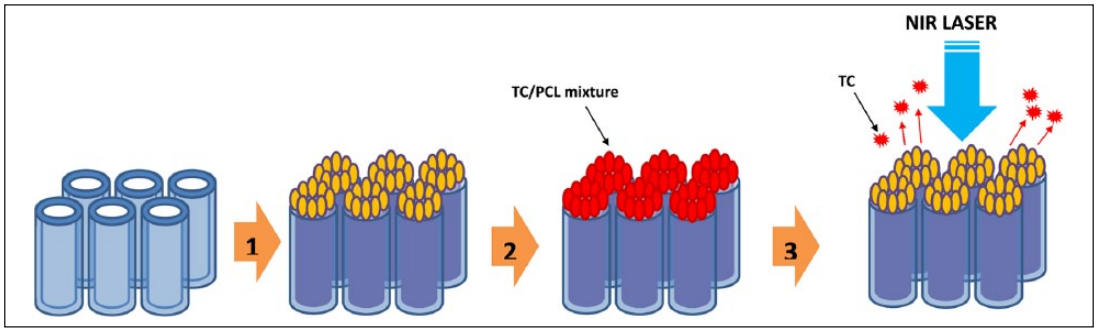

Figure 1. Schematic diagram of the preparation of the TC/PCL-coated GNRs-TiO_2 nanotube drug release system. (1) Gold nanoparticle sputtering onto TiO_2 nanotubes. (2) TC/PCL mixture coating on GNRs-TiO_2 nanotubes by electrospinning. (3) Remote-controlled TC release by NIR laser irradiation.

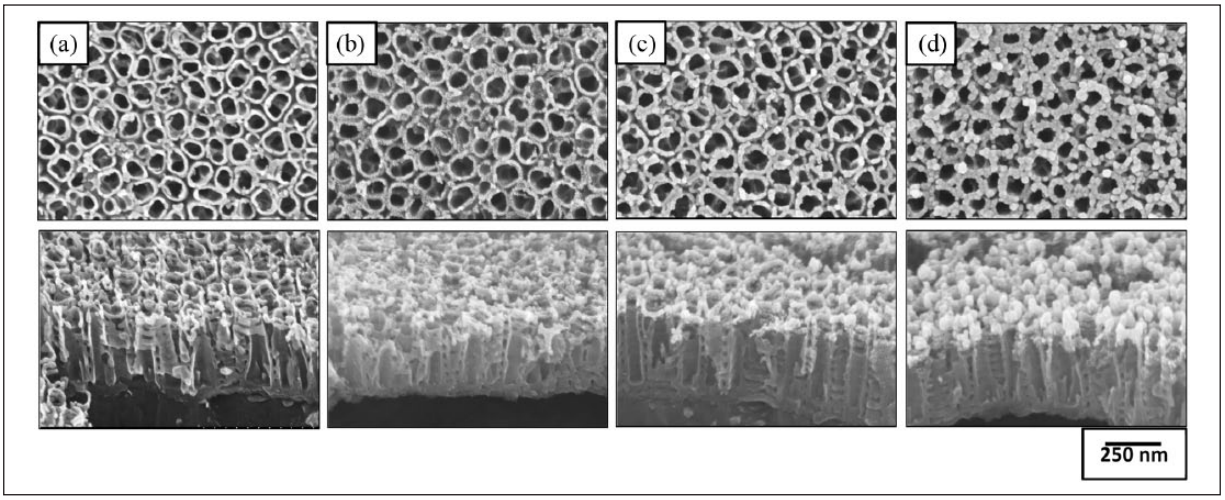

Figure 2. FE-SEM images of (a) 100-nm TiO_2 nanotubes and GNRs-TiO_2 nanotubes with (b) 1 min, (c) 3 min, and (d) 5 min of gold sputtering (top: plain view, bottom: oblique view).

wavelengths of 500–600 nm and above 800 nm are the main peaks resulting from photothermal scattering of the short and long axes of deposited gold nanoparticles, respectively.[20] From the results of diffusive UV-Vis-NIR spectrophotometry, 5 min of gold sputtering was selected to perform on–off drug release and remote-controlled antimicrobial activity using an 830-nm NIR laser.

Figure 5 shows the XPS spectra of GNRs-TiO_2 nanotubes with various gold sputtering periods. As the gold coating time increased, the main peaks of Ti 2p and O 1s were shifted to lower binding energies. Compared with pure TiO_2 nanotubes, the Ti peaks of GNRs-TiO_2 nanotubes showed a small shift to lower binding energy, suggesting the reduction of titanium species by increased deposition of gold. In addition, the O 1s peak showed a shift to lower binding energy (530.9 eV → 529.0 eV) with gold embedment. These peaks are related to oxygen in the lattice and O_2^- ions.[21]

Figure 6 shows the FDA-stained images and viable cell numbers of hMSCs cultured on TC/PCL-coated GNRs-TiO_2 nanotubes with the TC concentrations of 2, 4, and 5 wt%. From the results of viable cell numbers, there were no significant differences between the experimental groups after 24 h of incubation. After 48 h of incubation, the number of hMSCs cultured on 2 wt% TC/PCL-coated GNRs-TiO_2 nanotubes was significantly higher than that on 4 and 5 wt% TC/PCL-coated GNRs-TiO_2 nanotubes ($P < 0.05$).

Figure 7 shows the results of MTT cytotoxicity tests of hMSCs after 24 and 48 h of incubation. There were no significant differences between the experimental groups after 24 h of incubation. After 48 h of hMSC incubation, the viability of cells grown with 2 wt% TC/PCL-coated GNRs-TiO_2 nanotubes (70.74% ± 8.55%) was significantly higher than that of cells grown with 4 wt% (46.51% ± 3.65%) and 5 wt% (46.29% ± 10.53%) TC/PCL-coated GNRs-TiO_2 nanotubes ($P < 0.05$). In addition, the viability of cells grown with 2 wt% TC/PCL-coated GNRs-TiO_2 nanotubes was above 70% of the control (blank), implying that the nanotubes did not show cytotoxicity at a TC/PCL concentration of 2 wt%.[19]

Figure 8 presents the zone index results of antibacterial agar diffusion tests with 2 wt% TC/PCL-coated GNRs-TiO_2

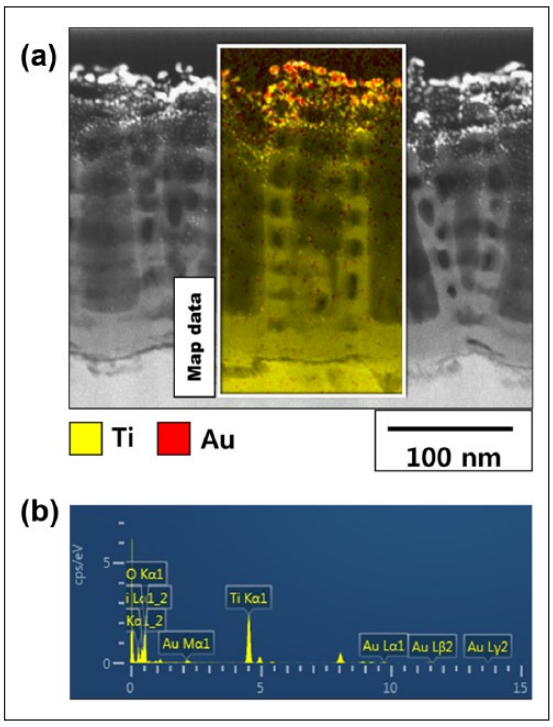

Figure 3. (a) TEM images and (b) EDX analysis of GNRs-TiO_2 nanotubes (5 min of gold sputtering).

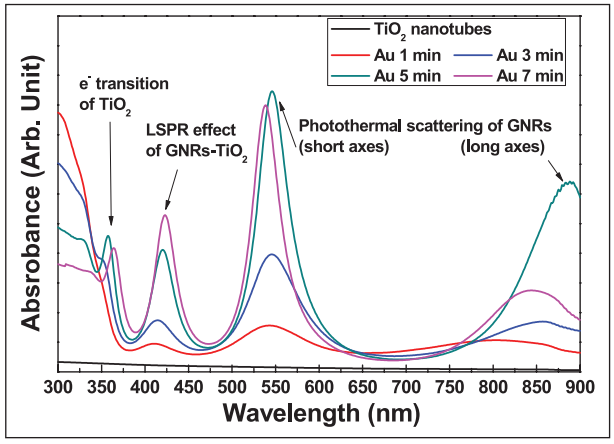

Figure 4. Diffuse UV-Vis-NIR spectrophotometry results of GNRs-TiO_2 nanotubes with various gold sputtering periods.

nanotubes after 1 min of NIR laser irradiation. The zone index of *S. mutans* grown with 2 wt% TC/PCL-coated GNRs-TiO_2 nanotubes following NIR laser irradiation for 1 min (16.25 ± 1.39 cm) was significantly higher than that of colonies grown with nanotubes without NIR laser irradiation (11.37 ± 0.52 cm; $P < 0.05$).

Finally, Figure 9 illustrates the LC-MS/MS results of mouse blood plasma following the injection of mice with 2 wt% TC/PCL-coated GNRs-TiO_2 nanotubes with or without NIR laser irradiation. The released amount of TC from 2 wt% TC/PCL-coated GNRs-TiO_2 nanotubes with NIR laser irradiation for 1 min (159.19 ± 25.16 ng/mL) was significantly higher than that of the nanotubes without NIR laser irradiation (100.50 ± 9.12 ng/mL; $P < 0.05$).

Discussion

The production of GNRs capable of selective drug elution by NIR laser irradiation was performed by sputtering in this study. Based on the FE-SEM and TEM observations, the gold nanoparticles were deposited on the top surface rather than the inner surface of the TiO_2 nanotubes and changed into the shape of nanorods as the deposition time of gold nanoparticles increased. In addition, the aspect ratio of the deposited GNRs reached a maximum of 1:3 after 5 min of deposition. Notably, the shape of the deposited nanoparticles was altered because of the directionality of the deposition of the nanoparticles during sputtering compared with chemical coating of pre-synthesized gold nanoparticles.[22,23] Moreover, most of the GNRs were observed in the uppermost layer of TiO_2 nanotubes, which could lead to more effective induction of the photothermal effect by NIR laser irradiation, unlike our previous experiments in which GNRs were evenly distributed throughout the nanotubes.[13] Also, the amount of Au deposited onto the surface of TiO_2 nanotubes was 36.50 ± 1.31 wt% as measured by EDX analysis (data not shown), which is approximately three times higher than that of Au coated onto the surface of TiO_2 nanotubes in our previous study.[13]

From the four peaks of diffuse UV-Vis-NIR spectra of GNRs-TiO_2 nanotubes with various gold sputtering periods shown in Figure 4, adsorption in the ultraviolet (UV) region (<400 nm) corresponds to electrons transitioning from the valence band to the conduction band of TiO_2.[24,25] The absorbance peak at around 425 nm was supposed to be the localized surface plasmon resonance (LSPR) effect of GNRs-TiO_2 nanotubes, because Au nanoparticles deposited on TiO_2 nanotubes serve as a stepping stone to electron transition from the valence to the conduction band of TiO_2 and extend the photocatalytic effect to the visible light region.[26,27] Two absorption peaks at the wavelengths of 500–600 nm and above 800 nm are the main peaks resulting from photothermal scattering of the short and long axes of the deposited gold nanoparticles, respectively.[20] The existence of gold nanoparticles in the form of nanorods was again identified by the results of diffuse UV-Vis-NIR spectrophotometry, showing strong absorption peaks at around 530 nm and above 800 nm. These two main peaks related to GNRs were already reported by other researchers in previous studies,[28–30] demonstrating that rod-shaped gold nanoparticles showed two surface plasmon bands composed of transverse and longitudinal plasmon bands. The transverse plasmon band was also shown to shift to a lower wavelength, and the longitudinal plasmon band moved to a higher wavelength as the aspect ratio of gold nanoparticles increased.[31] Therefore, the

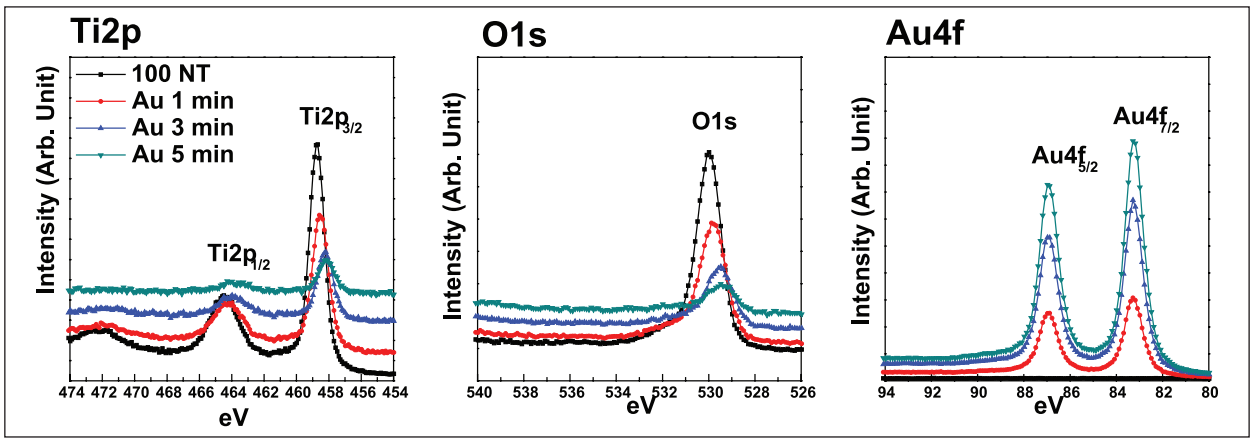

Figure 5. XPS spectra of GNRs-TiO_2 nanotubes with various gold sputtering periods.

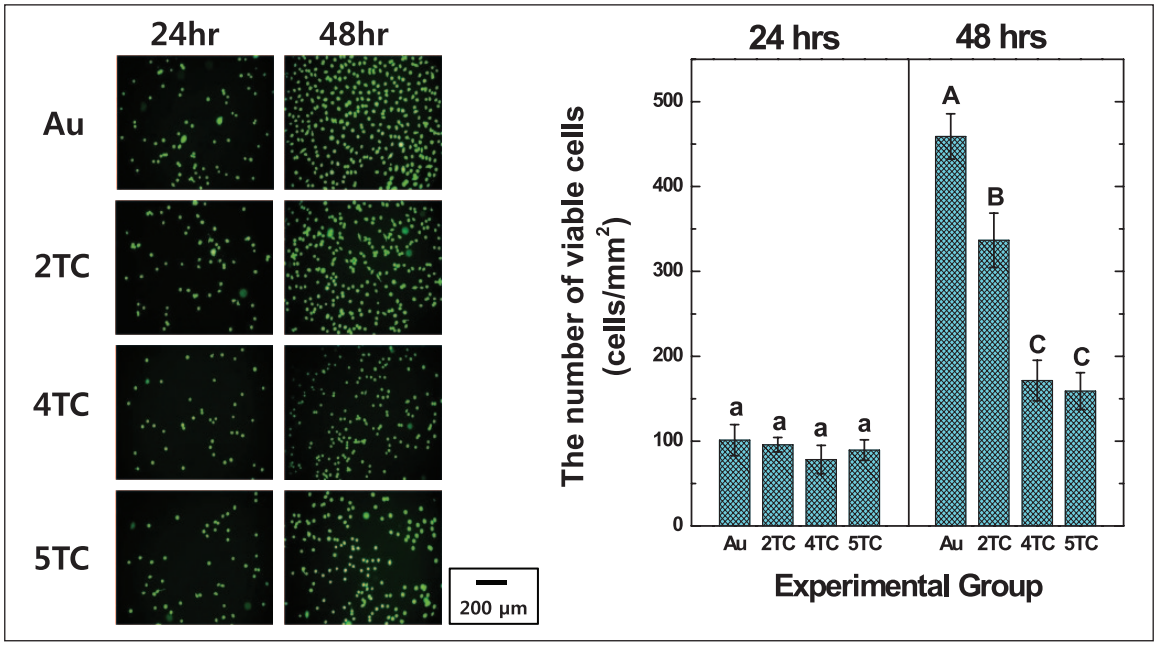

Figure 6. FDA-stained images and the number of viable hMSCs cultured on GNRs-TiO_2 nanotubes and 2, 4, and 5 wt% TC/PCL-coated GNRs-TiO_2 nanotubes (entries with the same uppercase and lowercase letters were not significantly different by one-way ANOVA at $\alpha = 0.05$).

maximum absorption wavelength shifted to a longer wavelength as the size of gold nanoparticles increased. In this experiment, gold sputtering for 5 min was selected for further analysis to maximize the photothermal effects of gold nanoparticles in the NIR region.

From the results of XPS spectra of GNRs-TiO_2 nanotubes with various gold sputtering periods, the main peaks of Ti 2p and O 1s were shifted to lower binding energies as the gold coating time increased. The shift of Ti peaks is related to the reduction of titanium species by increased deposition of gold. Also, the shift of O peaks is related to the oxygen in the lattice and O_2^- ions.[21] Thus, the shift of these major peaks to lower binding energy with gold embedment suggested increased defective or incomplete Ti–O binding with increased gold addition.[32]

In terms of NIR laser device used in this experiment, low-level 830-nm NIR laser is well known to be widely used for low-level laser therapy (LLLT) in medical use (e.g., the release of skeletal muscle fatigue,[33] the treatment of chronic neck pain,[34] tissue repair,[35] and bone repair[36]). Thus, 830-nm NIR laser was expected to show multifunctional effects with osseointegration and antibacterial activity. Also, we prepared TC/PCL mixture to control the release of TC and store TC effectively in an aqueous solution for a long time. FDA staining, MTT cytotoxicity tests, and antibacterial agar diffusion tests

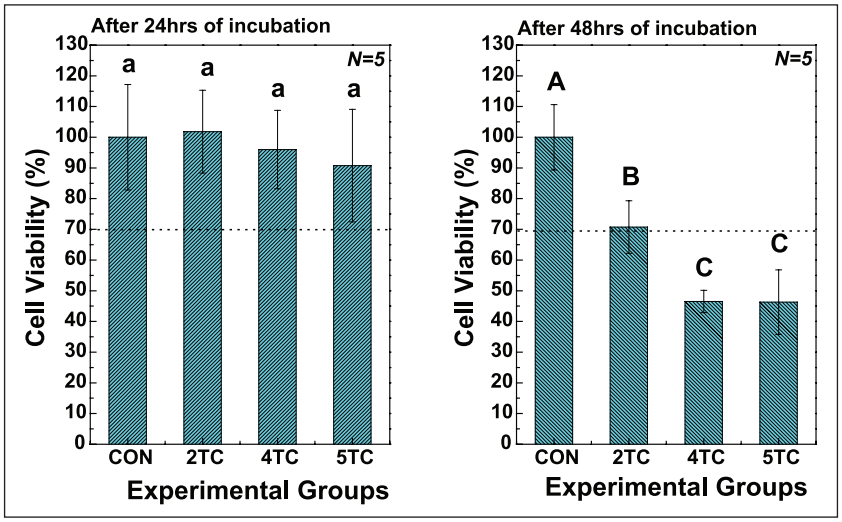

Figure 7. MTT assay results for GNRs-TiO_2 nanotubes and 2, 4, and 5 wt% TC/PCL-coated GNRs-TiO_2 nanotubes after 24 and 48 h of incubation with hMSCs (entries with the same uppercase and lowercase letters were not significantly different by one-way ANOVA at $\alpha = 0.05$).

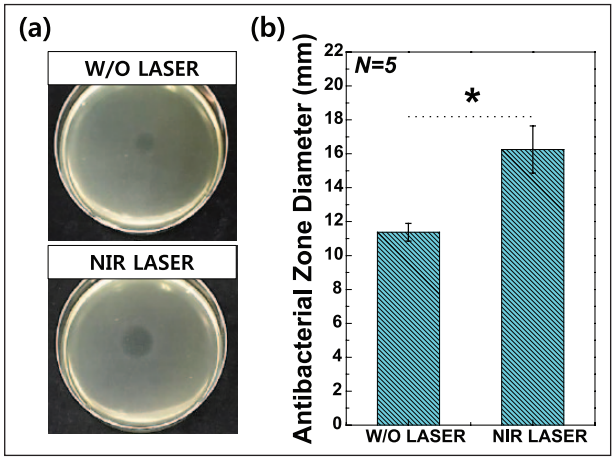

Figure 8. (a) Photographs of antibacterial agar diffusion tests using *Streptococcus mutans* and (b) results of zone diameter analysis for dead *Streptococcus mutans* in the presence of 2 wt% TC/PCL-coated GNRs-TiO_2 nanotubes without or with NIR laser irradiation for 1 min. All data were expressed as means ± standard deviations.
*significance between groups ($P < 0.05$).

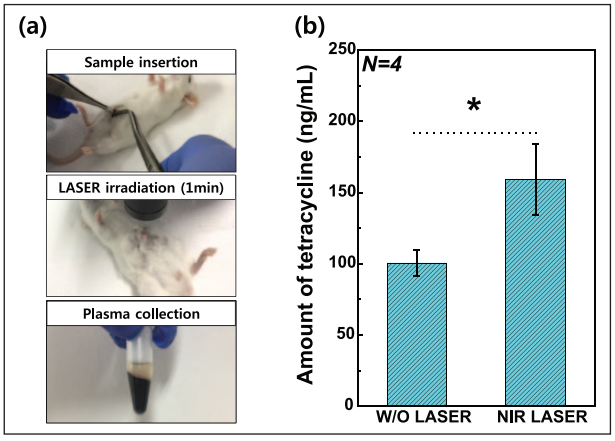

Figure 9. (a) Photographs of the experimental procedure of remote-controlled TC release tests in mice and (b) LC-MS/MS results for mouse blood plasma following the injection of 2 wt% TC/PCL-coated GNRs-TiO_2 nanotubes with or without NIR laser irradiation. All data were expressed as means ± standard deviations.
*significance between groups ($P < 0.05$).

were performed to determine the appropriate concentration of TC for inducing antimicrobial effects and maintaining biocompatibility. From the results of these tests, the 2 wt% TC/PCL experimental group was found to show only biocompatibility among all the experimental groups according to the requirement of ISO 10993-5. In addition, the results of LC-MS/MS measurement showed that the photothermal effects of GNRs deposited on the TiO_2 nanotubes could be used to detect the dissolution behaviors of antimicrobial drugs within 30 min in vivo following 1 min of NIR laser irradiation. Within the limitation of this study, GNR-sputtered TiO_2 nanotubes are expected to be a feasible new technology for the surface treatment of titanium-based implants.

Conclusion

From the results of this study, we found that GNR deposition on TiO_2 nanotubes can be performed successfully using a simple sputtering technique. Moreover, we confirmed that the TC/PCL mixture stored in GNRs-TiO_2 nanotubes was released effectively by NIR laser irradiation due to the photothermal effects of GNRs. Therefore, we

concluded that GNRs-TiO_2 nanotubes prepared using sputtering could extend the limited use of TiO_2 nanotubes from the UV to the NIR region, thereby facilitating the development of novel surface treatments in the field of implants.

Declaration of conflicting interests

The author(s) declared no potential conflicts of interest with respect to the research, authorship, and/or publication of this article.

Funding

The author(s) disclosed receipt of the following financial support for the research, authorship, and/or publication of this article: This research was supported by Basic Science Research Program of the National Research Foundation of Korea (NRF) funded by the Ministry of Education (2014R1A1A2053809 and 2016R1D1A1B03930607).

ORCID iD

Seunghan Oh https://orcid.org/0000-0002-7250-721X

References

1. Snauwaert K, Duyck J, van Steenberghe D, et al. Time dependent failure rate and marginal bone loss of implant supported prostheses: a 15-year follow-up study. *Clin Oral Investig* 2000; 4: 13–20.
2. Park JH, Olivares-Navarrete R, Baier RE, et al. Effect of cleaning and sterilization on titanium implant surface properties and cellular response. *Acta Biomater* 2012; 8: 1966–1975.
3. Gürsel I, Korkusuz F, Türesin F, et al. In vivo application of biodegradable controlled antibiotic release systems for the treatment of implant-related osteomyelitis. *Biomaterials* 2001; 22: 73–80.
4. Yuan A, Huan W, Liu X, et al. NIR light-activated drug release for synergetic chemo-photothermal therapy. *Mol Pharm* 2017; 14: 242–251.
5. Fu XD, Wang XJ, Zhou SL, et al. IONP-doped nanoparticles for highly effective NIR-controlled drug release and combination tumor therapy. *Int J Nanomedicine* 2017; 12: 3751–3766.
6. Yan F, Duan W, Li Y, et al. NIR-laser-controlled drug release from DOX/IR-780-loaded temperature-sensitive-liposomes for chemo-photothermal synergistic tumor therapy. *Theranostics* 2016; 6: 2337–2351.
7. Qiu M, Wang D, Liang W, et al. Novel concept of the smart NIR-light-controlled drug release of black phosphorus nanostructure for cancer therapy. *Proc Natl Acad Sci U S A* 2018; 115: 501–506.
8. Huang X, Neretina S and El-Sayed MA. Gold nanorods: from synthesis and properties to biological and biomedical applications. *Adv Mater* 2009; 21: 4880–4910.
9. Terentyuk GS, Ivanov AV, Polyanskaya NI, et al. Photothermal effects induced by laser heating of gold nanorods in suspensions and inoculated tumours during in vivo experiments. *Quantum Electron+* 2012; 42: 380–389.
10. Mooney R, Schena E, Saccomandi P, et al. Gold nanorod-mediated near-infrared laser ablation: in vivo experiments on mice and theoretical analysis at different settings. *Int J Hyperthermia* 2017; 33: 150–159.
11. Zhang S, He X, Dong S, et al. Study on the photo-thermal effect of gold nanorods irradiated with near infrared region laser in different conditions. *Sheng Wu Yi Xue Gong Cheng Xue Za Zhi* 2015; 32: 821–825.
12. Zhang Z, Wang J, Nie X, et al. Near infrared laser-induced targeted cancer therapy using thermoresponsive polymer encapsulated gold nanorods. *J Am Chem Soc* 2014; 136: 7317–7326.
13. Moon K-S, Bae J-M, Jin S, et al. Infrared-mediated drug elution activity of gold nanorod-grafted TiO_2 nanotubes. *J Nanomater* 2014; 2014: 750813.
14. Yi Y-A, Park Y-B, Choi H, et al. The evaluation of osseointegration of dental implant surface with different size of TiO_2 nanotube in rats. *J Nanomater* 2015; 2015: 581713.
15. Kang C-G, Park Y-B, Choi H, et al. Osseointegration of implants surface-treated with various diameters of TiO_2 nanotubes in rabbit. *J Nanomater* 2015; 2015: 634650.
16. Oh S, Brammer KS, Li YS, et al. Stem cell fate dictated solely by altered nanotube dimension. *Proc Natl Acad Sci U S A* 2009; 106: 2130–2135.
17. Brammer KS, Oh S, Cobb CJ, et al. Improved bone-forming functionality on diameter-controlled TiO_2 nanotube surface. *Acta Biomater* 2009; 5: 3215–3223.
18. Shin Y and Lee S. Self-organized regular arrays of anodic TiO_2 nanotubes. *Nano Lett* 2008; 8: 3171–3173.
19. ISO 10993-5:2009. Biological evaluation of medical devices: part 5: tests for in vitro cytotoxicity.
20. Chen YS, Frey W, Kim S, et al. Enhanced thermal stability of silica-coated gold nanorods for photoacoustic imaging and image-guided therapy. *Opt Express* 2010; 18: 8867–8878.
21. Nagasawa Y, Choso T, Karasuda T, et al. Photoemission study of the interaction of a reduced thin film SnO2 with oxygen. *Surf Sci* 1999; 433–435: 226–229.
22. Mahshid S, Li C, Mahshid SS, et al. Sensitive determination of dopamine in the presence of uric acid and ascorbic acid using TiO_2 nanotubes modified with Pd, Pt and Au nanoparticles. *Analyst* 2011; 136: 2322–2329.
23. Zhang Z, Zhang L, Hedhili MN, et al. Plasmonic gold nanocrystals coupled with photonic crystal seamlessly on TiO_2 nanotube photoelectrodes for efficient visible light photoelectrochemical water splitting. *Nano Lett* 2013; 13: 14–20.
24. Gu D, Wang YC, Li Z, et al. UV-light aided photoelectrochemical synthesis of Au/TiO_2 NTs for photoelectrocatalytic degradation of HPAM. *RSC Adv* 2016; 6: 63711–63716.
25. Xiao F-X, Hung S-F, Miao J, et al. Metal-cluster-decorated TiO_2 nanotube arrays: a composite heterostructure toward versatile photocatalytic and photoelectrochemical applications. *Small* 2015; 11: 554–567.
26. Yoo SM, Rawal SB, Lee JE, et al. Size-dependence of plasmonic Au nanoparticles in photocatalytic behavior of Au/TiO_2 and Au@SiO_2/TiO_2. *Appl Catal A: Gen* 2015; 499: 47–54.
27. Lin ZJ, Wang XH, Liu J, et al. On the role of localized surface plasmon resonance in UV-Vis light irradiated Au/TiO_2 photocatalysis systems: pros and cons. *Nanoscale* 2015; 7: 4114–4123.

28. Khlebtsov BN and Khlebtsov NG. Multipole plasmons in metal nanorods: scaling properties and dependence on particle size, shape, orientation, and dielectric environment. *J Phys Chem C* 2007; 111: 11516–11527.
29. Liao Q, Mu C, Xu DS, et al. Gold nanorod arrays with good reproducibility for high-performance surface-enhanced Raman scattering. *Langmuir* 2009; 25: 4708–4714.
30. Zhang K, Xiang Y, Wu X, et al. Enhanced optical responses of Au@Pd core/shell nanobars. *Langmuir* 2009; 25: 1162–1168.
31. Kim S, Shuford KL, Bok H-M, et al. Intraparticle surface plasmon coupling in quasi-one-dimensional nanostructures. *Nano Lett* 2008; 8: 800–804.
32. Vuong NM, Kim D and Kim H. Porous Au-embedded WO3 nanowire structure for efficient detection of CH4 and H2S. *Sci Rep* 2015; 5: 11040.
33. Leal Junior EC, Lopes-Martins RA, Vanin AA, et al. Effect of 830 nm low-level laser therapy in exercise-induced skeletal muscle fatigue in humans. *Lasers Med Sci* 2009; 24: 425–431.
34. Chow RT, Heller GZ and Barnsley L. The effect of 300 mW, 830 nm laser on chronic neck pain: a double-blind, randomized, placebo-controlled study. *Pain* 2006; 124: 201–210.
35. Oliveira FS, Pinfildi CE, Parizoto NA, et al. Effect of low level laser therapy (830 nm) with different therapy regimes on the process of tissue repair in partial lesion calcaneous tendon. *Lasers Surg Med* 2009; 41: 271–276.
36. Bossini PS, Rennó AC, Ribeiro DA, et al. Low level laser therapy (830 nm) improves bone repair in osteoporotic rats: similar outcomes at two different dosages. *Exp Gerontol* 2012; 47: 136–142.